Raman Spectroscopy and Electrochemical Analysis of the Corrosion Behaviour of Reinforcing Steel in the Presence of TEE as an Inhibitor

Zhikun Li[1,2,] and Jiahui Peng[1]*

[1] College of Materials Science and Engineering of Chongqing University, Chongqing, 400030, P.R. China
[2] Chongqing Research Institute of Building Science, Chongqing, 400020, P.R. China
[*]E-mail: pengjiahui@yahoo.com

Using techniques such as in situ and ex situ Raman spectroscopy, cyclic voltammetry (CV), open-circuit potential (OCP) and electrochemical impedance spectroscopy (EIS), this work explored steel corrosion and its inhibition by Tagetes erecta (Marigold flower) in 3.5% NaCl solutions. As indicated by the electrochemical analysis, a reduced corrosion rate and corrosion current density as well as more positive corrosion potential values were obtained by adding and increasing the concentration of the Tagetes erecta extract (TEE). When the immersion time of an iron electrode in the test electrolyte was lengthened to 24 h, the abovementioned effect was strengthened. Using the Raman method, it was verified that iron corrosion was significantly inhibited by the obstruction of the iron active sites via the adsorption of TEE extract onto its surface when present in the chloride solution.

1. INTRODUCTION

Reinforcing steel is among the most frequently used construction materials for strengthening concrete structures and therefore makes a remarkable contribution to the development of the economy. Nevertheless, on a global scale, the corrosion of reinforcing steel is an important issue because it is a main cause of the premature degradation of concrete structures [1-3]. Thus, there is an urgent need for contemporary research on the mechanisms of corrosion as well as on the protection of steel. Typically, a passive film is generated on the surface of steel within concrete pore solutions that typically have a significantly alkaline pH of 12.0 to 13.0, thus inhibiting the corrosion of the reinforcing steel in concrete. It is believed that the passive oxide film is thin with a certain adherence and that it inhibits

corrosion through the generation of an Fe_2O_3 layer on the surface [4]. Nevertheless, both the chemical and physical conditions at the interface between the media and the steel determine whether the passivity of the steel lasts. When the critical chloride concentration and/or pH value for corrosion at the interface between the concrete and steel is achieved, the reinforcing steel will corrode due to damage of the protective film [5-11].

A popular hypothesis is that the dissolution of metals can be prevented via eliminating the unfavourable and destructive effects of the aggressive media through the use of corrosion inhibitors. Most of the inhibition occurs when the inhibitor adsorbs onto and interacts with the surface of the iron [12-14]. In addition to the adsorption mechanism, the relations between the adsorption traits and the various forms of organic corrosion inhibitors are also a consideration for researchers. Polymeric complexes can be generated on the surfaces of metals, in which azole derivatives, such as benzimidazole, benzotriazole, imidazole, and mercaptobenzothiazole, all popular corrosion inhibitors, are adsorbed onto the surface. Conversely, a protective film can also be adhered onto a metal and obstruct interactions with aggressive ions such as chloride [15]. Based on previous literature, heterocyclic compounds containing conjugated double bonds and polar functional groups generally exhibit good inhibition performance, as do organic compounds with polar groups, including nitrogen, oxygen, phosphorus, and sulfur [16-20]. Such organic compounds interact with the surface of the metal where they are adsorbed, which accounts for most of the inhibition. Stable adsorption is concentrated at the functional polar groups, which are known as the centres of the reaction. Nevertheless, on the surface of a metal, several factors, including the chemical structure of the protective inhibitor, surface charge of the metal, traits of the metal, type of electrolyte solution, and mode of adsorption, determine the inhibitor adsorption.

Raman spectroscopy has been used to study metallic corrosion performance for approximately 20 years [18, 21, 22]. However, for a large number of important transition metals, traditional Raman spectroscopy is not sufficiently sensitive to examine monolayers on their surfaces. Furthermore, they do not exhibit surface-enhanced Raman phenomena. In situ research concerning electrochemical molecular-level processes of metals can be conducted using surface-enhanced Raman spectroscopy (SERS). SERS excels in both transient and steady-state approaches to conventional electrochemical techniques [23]. Only a small SERS effect is observed for Fe, a metallic material that is widely utilized. Fe corrosion has been studied using several techniques in order to fully analyse substrates of Fe using SERS [24, 25]. Among these techniques, enhanced Fe Raman spectra have been obtained using electrodeposition approaches such as the deposition of a thin Fe layer on a Raman-active Au surface, developed by Joiret and Allongue [24], and the deposition of Raman-active Ag on the surface of Fe, developed by Melendres and co-workers [25]. SERS-active Fe surfaces can be roughened using electrochemical roughening approaches, including redox cycling, electrochemical oxidation or etching. Nevertheless, in terms of Fe performing the role of a substrate for reinforcing steel, these approaches are not advantageous for comprehensively investigating the corrosion performance. Moreover, the spectra are difficult to analyse due to interference from the Raman-active metals, and the real state of the reinforcing steel is not reflected because the Fe surfaces must be roughened. Thus, the processes of in situ corrosion have been investigated on original Fe surfaces by dedicated corrosion experts using Raman spectroscopy. Herein, improvements to these methods are reported. Using

applied potentials within a certain range, model iron electrodes have been characterized successfully by Larroumet and coworkers via unenhanced Raman spectroscopy in a neutral solution [22]. In this study, Raman spectroscopy was employed to investigate corrosion and carbon steel corrosion inhibition in 3.5% NaCl solutions, and the results are discussed. In addition to Raman techniques, methods such as chronoamperometry (CA), cyclic voltammetry (CV), electrochemical impedance spectroscopy (EIS), open-circuit potential (OCP), and potentiodynamic polarization (PDP) were adopted for electrochemical analyses.

2. EXPERIMENTS

2.1. Materials

R235 reinforcing steel containing C (0.390), Cu (0.101) Mn (0.254), Ni (0.027), P (0.015), S (0.012), Si (0.083) (wt.%) and the balance of Fe was designated as the target material, which was processed into cylinder-shaped samples of $\varnothing 1.13$ cm $\times$ 0.4 cm via cutting. Subsequently, the sample surfaces were subjected to SiC paper polishing, double-distilled water washing, ultrasonic ethanol cleaning and air drying. For the electrochemical experiments, the as-prepared samples were embedded in a PVC holder after being processed through epoxy resin sealing, leaving 1.00 cm^2 of its working surface exposed.Marigold petals were de-plucked from rest of the flower. The petals were dried in tray drier at 50 °C. The colorants of petals were extracted with 100 mL of aqueous ethanol (60:40) using Soxhlet apparatus. 10 g of dry petals were refluxed for 1 h. After complete extraction, the solvent was evaporated and then dried to get solid mass. About 0.5 g TEE solid can be collected from 10 g petals.

2.2. Raman analysis

In situ Raman analysis was conducted using a Teflon cell. An iron rod with a 9.5-mm diameter was employed as the source of a thick disc (2 mm), which was cut with a diamond rotary blade. The disc from the iron rod was subjected to polishing and cleaning. Any surface heating induced by the laser was prevented with pre-emptive surface cooling, which was achieved by flowing electrolyte over the surface using a peristaltic pump. The circulation of the electrolyte was possible due to the special design of the cell. Before being positioned 2 mm from the surface of the iron, a Ag/AgCl reference electrode was connected to a Lugging probe with an inner diameter of 0.5 mm. With an outside diameter of 10 mm and a thickness of 0.2 mm, a Pt ring disc was employed as the counter electrode and positioned 2 mm above the surface of the iron. A JY T64000 Raman spectrometer was used in single spectrograph mode. Featuring a long working distance 20× objective, an Olympus confocal microscope attached to the spectrometer was used to analyse the surface of the iron in the electrochemical cell on the stage of the microscope in back-scattering mode. A charge-coupled device (CCD) detector modified with liquid nitrogen cooling was employed for detection.

2.3. Electrochemical analysis

Prior to the electrochemical experiments, which were conducted with an electrochemical system, the iron electrode was immersed for 1 or 24 h in a 3.5% NaCl solution both with and without TEE (0.47, 0.94, and 1.88 g/L). The CV of the iron electrode that was immersed for 1 h either with or without the addition of the TEE extract was scanned at a rate of 1 mV/s. Potentiostatic current–time experiments were carried out by stepping the potential at −500 mV for 120 min. EIS tests were conducted at certain corrosion potentials (E_{corr}) at frequencies ranging between 100 and 0.1 Hz. All of the measurements were recorded at ambient temperature. Ethanol (99:1, vol:vol) and double-distilled water were employed for all solutions.

2.4 Corrosion rate calculation

The corrosion rate (K_{Corr}, millimetres per year (mmy^{-1})) was calculated using the following equation: $K_{Corr} = \dfrac{j_{Corr}kE_w}{dA}$

where k is a constant that defines the units of the corrosion rate (=3272 mm/cm/year), E_W is the equivalent weight in grams/equivalent of pure iron (=27.93), d the density in g/cm^3 (=7.86), and A is the exposed area of the electrode surface in cm^2.
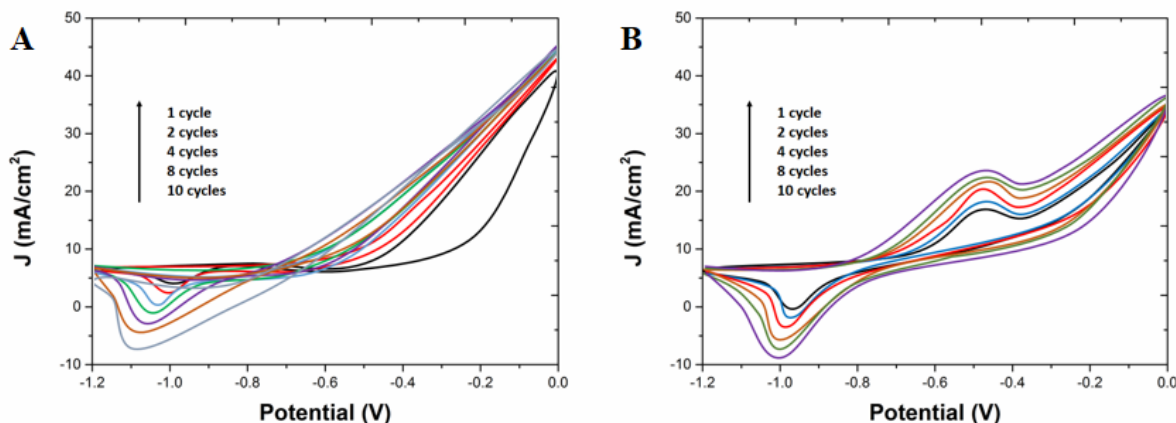
3. RESULTS AND DISCUSSION

Figure 1. Cyclic voltammograms of the iron electrode in solutions of (A) 3.5% NaCl and (B) 3.5% NaCl containing 0.47 g/L TEE.

The iron electrode in an aerated 3.5% NaCl solution was characterized with and without the addition of TEE (0.47 g/L) through the CV curves depicted in Figure 1. Figure 1A displays an obvious anodic and cathodic peak. Specifically, the anodic peak appeared in the Cycle 5 at approximately -

540 mV, while the cathodic peak was observed at approximately -970 mV in Cycle 1. As the cycling progressed, the peaks shifted to approximately 1105 and -500 mV, respectively. The peaks represent the first oxidation of Fe to $Fe(OH)_2$. The reduction peak is not well defined in a few scans because it is masked by hydrogen evolution [26]. Meanwhile, as seen in Figure 1B, after ten cycles during the experiment in which TEE was added, the cathodic peak shifted to approximately -1010 mV, and the anodic peak shifted to approximately -470 mV, which reveals that the cathodic and anodic reactions on the surface of the iron were sensitive to the addition of TEE. The decrease in the overpotential of the oxidation peak was ascribed to the role of magnetite during passive film formation in the TEE-containing solution [10].
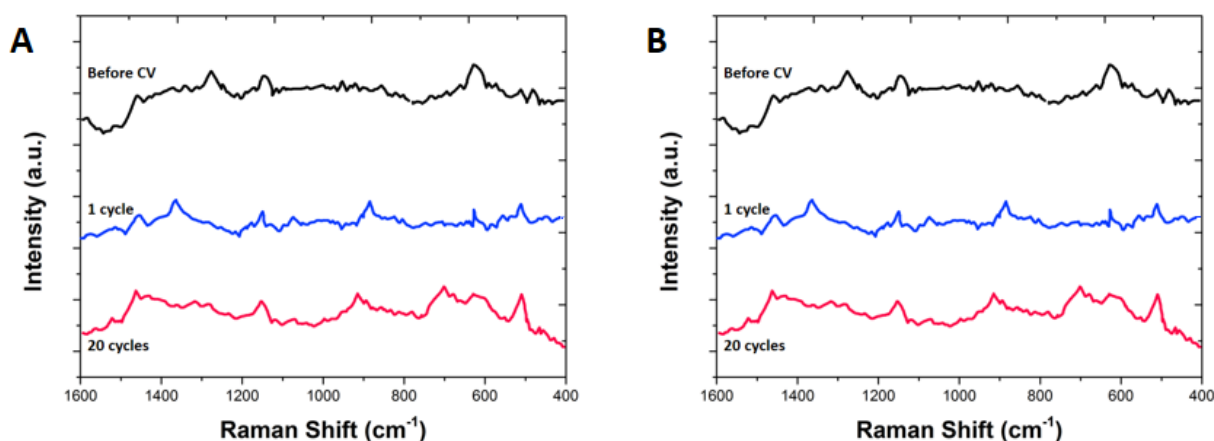

Figure 2. Raman spectra obtained on the iron surface before and after the 1st and 10th CV cycles in a 3.5% NaCl solution in the (A) absence and (B) presence of 0.47 g/L TEE.

In situ Raman analyses were conducted on the iron electrode surface before and after Cycle 1 and Cycle 10 following immersion for 60 min in a 3.5% NaCl solution either with or without the addition of TEE (0.47 g/L), and the data are displayed in Figure 2. Due to the high relative humidity of 80% and resulting matrix effects of the atmosphere, the signal-to-noise ratio and the shape of the Raman signals are of minor quality and bands below 400 cm^{-1} are not assigned to Raman signals [27]. As shown in Figure 2, even after 10 cycles, only weak bands were observed for iron in the chloride solutions. As the Fe^{2+} that is generated in the process of corrosion is oxidized, the Fe^{3+}–OH_2 bond vibrates, thus leading to a 491 cm^{-1} band. In comparison, with no potential applied, a strong band can be observed at 877 cm^{-1} for the iron in the TEE chloride solution. The 877 cm^{-1} band shifted to 871 cm^{-1} after Cycle 1. As the sample progressed to Cycle 10, the intensity of this band increased. The curves in the CV were characterized by other bands at 631, 1051, 1072, 1279, and 1452 cm^{-1}. Such bands occurred when TEE was added, which revealed significant surface adsorption and the subsequent polymerization of TEE. Triazole ring torsion accounts for the band at 631 cm^{-1}, and triazole ring breathing accounts for the band at 871 cm^{-1}. The bands at 1051, 1072, 1279 and 1452 cm^{-1} could be explained by the in-plane triazole ring-stretching vibrations of the TEE$^-$ anions

that interact with Fe(II), –N══N– stretching, CH in-plane bending and triazole ring stretching, respectively. The data demonstrate the reaction process of the corrosion in the presence of chloride ions [28]. The fact that four distinct hydroxyl stretching vibrations were observed in the hydroxyl-stretching region of the Raman spectra implies that four bands should also have been observed in the hydroxyl deformation region [29] because the extent of adsorption and the resultant coverage by the inhibitor on the steel surface increased with the inhibitor concentration [29, 30].

After stepping the potential to -600 mV and -1050 mV, an in situ Raman analysis of the iron surface after Cycle 1 and Cycle 10 in 3.5% NaCl with and without TEE (0.47 g/L) was conducted because the potential of the electrode determines the formation of the complex with amino-triazole, and the spectra are displayed in Figure 3. As revealed in the spectrum in Figure 3A, the major Raman peaks after Cycle 1 occurred at 877, 1049, 1113, and 1308 cm^{-1}. The spectrum obtained after Cycle 10 shows that the original peaks either vanished or intensified, and novel peaks appeared, which resulted from the oxidation of the Fe^{2+} that is produced during the corrosion processes [31]. Figure 3B indicates that the band at 881 cm^{-1} intensified and shifted to 865 cm^{-1}, which is typical of N–H bonding vibration and supports the hypothesis that the formation of Fe–N coordination bonds and deprotonation of the triazole ring may occur upon interactions between TEE with the iron surface [13]. During the interaction between the iron surface and TEE, it is likely that the triazole ring was deprotonated and that an Fe–N coordination bond was formed. The positions of these peaks were shifted, suggesting the formation of a modified hematite [32]. This presumption was confirmed by the absence of a peak at 1096 cm^{-1} in the Raman spectrum, which strongly suggests N–H bonding vibrations, as stated by Mennucci and co-workers [33]. The peak at 1209 cm^{-1} indicated the adsorption of biomolecules from the TEE extract onto the steel surface and the generation of a complex layer [34-37].
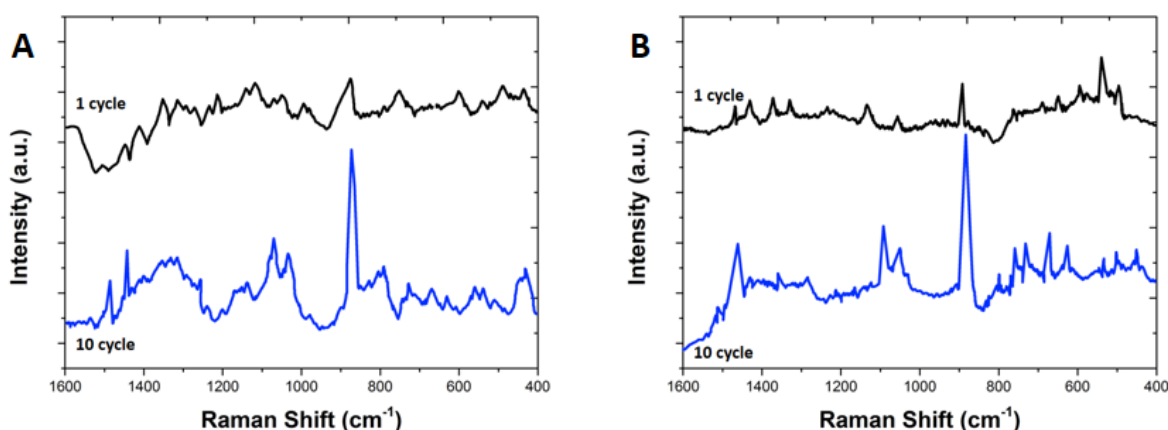

Figure 3. Raman spectra obtained on the iron surface in a 3.5% NaCl + 0.47 g/L TEE solution after the 1st and 10th CV cycles when the potential was stepped to (A) -600 mV or (B) -1050 mV.

In 3.5% NaCl solutions both with and without TEE (0.47, 0.94, and 1.88 g/L), the iron electrode was characterized using the OCP curves depicted in Figure 4. The invasion of chloride ions on the surface of the electrode caused the iron to dissolve, resulting in a lower negative potential in the

absence of TEE. Singh et al. [38] observed that the Raman spectrum presented significant noise when a laser power of less than 1.5 mW was used. El Mendili et al. [39] investigated the stability of the γ-Fe_2O_3 nanoparticles under laser irradiation with laser powers from 0.08 to 48 mW on the sample and thermal treatment (300–1400 °C). The partial protection of the iron against further serious invasions of chloride ions was achieved as corrosion products formed on the surface of the iron; thus, the longer periods of immersion caused small shifts in the positive direction. However, after immersing the electrode for 60 min, the potential moved in the positive direction upon the addition of TEE (0.5 mM). The presence of TEE and the increase in its concentration significantly decreased the anodic and cathodic corrosion currents as well as shifted the corrosion potential to more positive values, which was due to increasing the surface resistance of iron to corrosion. The effect was reduced as the curve exhibited minimal fluctuations with lengthened experiment durations. With longer immersion times (1 d), the OCP still shifted to more positive values after adding TEE (0.94, and 1.88 g/L). This result suggests that a stable Fe potential was achieved via the Fe-surface adsorption of TEE with increasing concentrations.
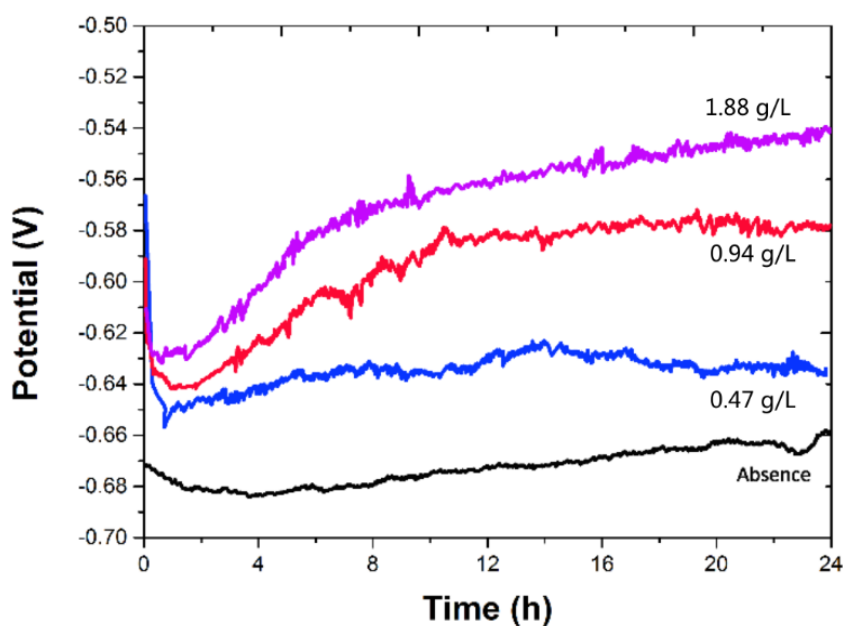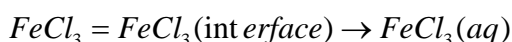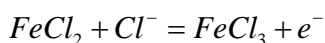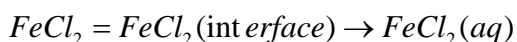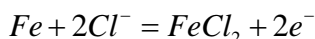

Figure 4. OCP curves for the iron electrode in 3.5% NaCl in the absence or presence of 0.47, 0.94, and 1.88 g/L TEE.

Following 1 and 24 h of immersion in a 3.5% NaCl solution with and without TEE (0.47, 0.94, and 1.88 g/L), the iron electrode was characterized using the current-time curves in Figure 5 prior to stepping the potential to -500 mV. For the Fe in the chloride solutions, the maximum currents were obtained without the addition of TEE, which predicts the formation of $FeCl_2$ and $FeCl_3$ mixed porous film(s) on the surface of the electrode. The type of iron phases formed was dependent on the type of alkaline solution used in the activation of fly ash and the amount of chloride added to the cementitious system [40]. At the interface, the solution was saturated with $FeCl_2$ and $FeCl_3$ since $FeCl_2$ and $FeCl_3$

precipitated and generated a film. The diffusion of the $FeCl_2$ and $FeCl_3$ groups through the porous film and the boundary layer occurred at the interface during the application of a potential that formed a concentration gradient. Subsequently, they were delivered to the bulk solution via convection. As the duration of the applied potential on the surface of iron increased, pitting corrosion occurred as the iron continued to dissolve.

The corrosion sites on the iron surface were significantly inhibited and obstructed by the TEE extract at the studied concentrations; thus, the absolute iron current was significantly reduced as TTE was added. The dissolution of iron under these conditions occurred according to the following reactions:

$$Fe + 2Cl^- = FeCl_2 + 2e^-$$
$$FeCl_2 = FeCl_2(\text{int} \, erface) \rightarrow FeCl_2(aq)$$
$$FeCl_2 + Cl^- = FeCl_3 + e^-$$
$$FeCl_3 = FeCl_3(\text{int} \, erface) \rightarrow FeCl_3(aq)$$

As the period of immersion was extended to 1 d and the concentration of TEE was increased, the effect became remarkably obvious and suggested that pitting corrosion would occur. This correspondingly proves that the extract of TEE were able to prevent corrosion and iron pitting through iron surface inhibition. The inhibition occurred because iron chlorides were not generated when TEE was added. Note that these iron chlorides performed the role of accelerating the iron corrosion. These chloride compounds have not been generated since the required concentration for Fe dissolution could not be reached with the insufficient anodic dissolution rate that occurred when TEE was added.
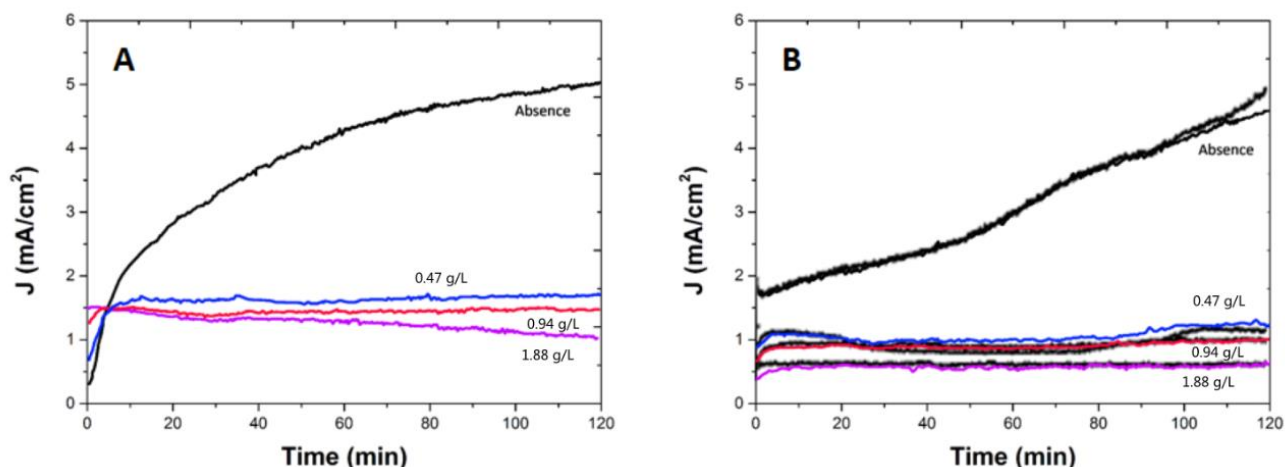

Figure 5. Potentiostatic current-time curves at -500 mV for iron electrodes in 3.5% NaCl in the absence or presence of 0.47, 0.94, and 1.88 g/L TEE after (A) 1 h and (B) 24 h.

The mechanisms of corrosion could easily be studied with the EIS method. The kinetic parameters for the electron shift reactions were determined by conducting an EIS analysis at the interface between the electrolyte and iron. EIS was also used to confirm the results of the polarization and chronoamperometric techniques in this work. The iron was characterized both with and without

the addition of TEE (0.47, 0.94, and 1.88 g/L) using the Nyquist plots in Figure 6, following immersion in a 3.5% NaCl solution for 1 h and 24 h. As indicated in Figure 6, with longer periods of immersion and without the addition of TEE in the chloride solution, an increase in the iron Rp and Rs values was observed due to the corrosion products that formed on the surface of the iron; as time passed, the iron became partially protected. As a result, the Rp value increased while the corrosion rate ($KCorr$) and corrosion current density ($jCorr$) decreased. The Rp and Rs values increased with the presence of TEE (0.47 g/L), and they continued to increase with longer immersion periods and increased concentrations of TEE.

Table 1. Ihibition efficiency of TEE at different concentrations.

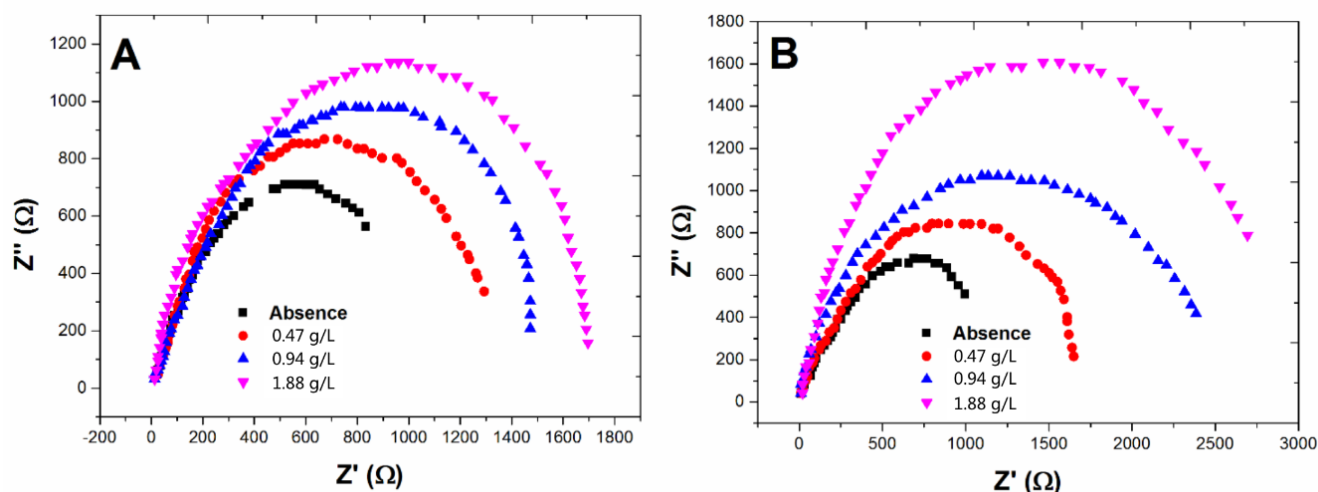| Concentration (mM)	Inhibition efficiency (%)
Blank	—
0.47 g/L	77%
0.94 g/L	91%
1.88 g/L	96%

Figure 6. Nyquist plots of the iron electrode at its open-circuit potential after immersion for (A) 1 h and (B) 24 h in 3.5% NaCl in the absence or presence of 0.47, 0.94, and 1.88 g/L TEE.

Double-layer porous capacitors were modelled using constant phase elements (CPEs, Q); the n values of which were approximately 1.0. As the concentration of TEE increased, the CPE values in the solution decreased as well as the capacitive effects and the charged surface coverage. In general, double-layer capacitor relaxation is related to high frequency semicircles (Figure 6), in which the diameters represent the charge transfer resistance (Rp). Generally, coinciding with the corrosion potential transfer, Rp experienced a stable increase with the increasing TEE concentration during the electron shift reaction. These results are in good agreement with precedent data published on dense corrosion product layer of steel embedded in concrete [41]. In the chloride solution, the Fe corrosion

was remarkably inhibited by TEE, which increased the IE%. The inhibition efficiency (η) was calculated using the following equation:

$$\eta = \frac{R_p - R_s}{R_p}$$

where R_p and R_s are the charge transfer resistance values in the uninhibited and inhibited solution, respectively. The fitting results reveal that R_p and R_s have maximum values of 0.07, 0.12 and 0.31 for 0.47, 0.94, and 1.88 g/L of TEE, respectively. The variations in the inhibition efficiency versus the TEE concentration that were obtained from the EIS analysis clearly demonstrate that the average inhibitive efficiency at different TEE concentrations occurred in the following sequence: 1.88 g/L > 0.94 g/L >0.47 g/L > Blank. Table 1 lists the calculated IE% values for each case.

4. CONCLUSIONS

Raman and electrochemical methods were employed to investigate steel corrosion in 3.5% NaCl with corrosion inhibition by TEE. The CV analysis revealed the presence of peaks with diverse potential values that arose from organic molecules on the iron surface that appeared upon the addition of TEE. As revealed by EIS, for the open-circuit potential and iron potentiostatic current-time in the target chloride solutions, the iron polarization resistance was boosted with the addition of TEE and with an increase in its concentration. However, the corrosion rate and current as well as the cathodic and anodic peaks were greatly reduced as a result. The extract of TEE were adsorbed onto the surface of iron through the formation of [TEE$^-$–Fe(II)] complexes, thus leading to the abovementioned shifts in potential peaks that were revealed by in situ Raman measurements.

References

1. V. Kumar, *Corrosion Reviews*, 16 (1998) 317.
2. S. Ahmad, *Cement and Concrete Composites*, 25 (2003) 459.
3. D. Hobbs, *International Materials Reviews*, 46 (2001) 117.
4. B. Huet, V. L'Hostis, F. Miserque and H. Idrissi, *Electrochimica Acta*, 51 (2005) 172.
5. Y. Ma, Y. Li and F. Wang, *Corrosion Science*, 51 (2009) 997.
6. K. Ann, J. Ahn and J. Ryou, *Construction and Building Materials*, 23 (2009) 239.
7. M. Montemor, A. Simoes and M. Ferreira, *Cement and Concrete Composites*, 25 (2003) 491.
8. R. Du, R. Hu, R. Huang and C. Lin, *Anal. Chem.*, 78 (2006) 3179.
9. Y. Sun, A. Shieh, S. Kim, S. King, A. Kim, H. Sun, C. Croce and J. Parquette, *Bioorganic & Medicinal Chemistry Letters*, 26 (2016) 2834.
10. S. Joiret, M. Keddam, X.R. Nóvoa, M.C. Pérez, C. Rangel and H. Takenouti, *Cement and Concrete Composites*, 24 (2002) 7.
11. Z. Yao, Y. Sun and C. Kang, *Nano LIFE*, 6 (2016) 1642007.
12. E. Sherif, *Appl. Surf. Sci.*, 252 (2006) 8615.
13. E. Sherif, R. Erasmus and J. Comins, *Electrochimica Acta*, 55 (2010) 3657.
14. E. Sherif and S. Park, *Electrochimica Acta*, 51 (2006) 1313.
15. V. Lakshminarayanan, R. Kannan and S. Rajagopalan, *Journal of Electroanalytical Chemistry*, 364 (1994) 79.
16. A. Chetouani, A. Aouniti, B. Hammouti, N. Benchat, T. Benhadda and S. Kertit, *Corrosion*

Science, 45 (2003) 1675.
17. P. Zhao, Q. Liang and Y. Li, *Appl. Surf. Sci.*, 252 (2005) 1596.
18. J. Yao, B. Ren, Z. Huang, P. Cao, R. Gu and Z.-Q. Tian, *Electrochimica Acta*, 48 (2003) 1263.
19. M. Bazzaoui, L. Martins, E. Bazzaoui and J. Martins, *Electrochimica Acta*, 47 (2002) 2953.
20. K. Zawada, J. Bukowska, M. Calvo and K. Jackowska, *Electrochimica Acta*, 46 (2001) 2671.
21. W. Baek, T. Kang, H. Sohn and Y. Kho, *Electrochimica Acta*, 46 (2001) 2321.
22. D. Larroumet, D. Greenfield, R. Akid and J. Yarwood, *Journal of Raman Spectroscopy*, 38 (2007) 1577.
23. B. Ren, G. Liu, X. Lian, Z. Yang and Z. Tian, *Anal Bioanal Chem*, 388 (2007) 29.
24. P. Allongue and S. Joiret, *Physical Review B*, 71 (2005) 115407.
25. C. Melendres, M. Pankuch, Y. Li and R. Knight, *Electrochimica Acta*, 37 (1992) 2747.
26. M. Cabrini, S. Lorenzi and T. Pastore, *Electrochimica Acta*, 124 (2014) 156.
27. P. Eckold, M. Rolff, R. Niewa and W. Hügel, *Corrosion Science*, 98 (2015) 399.
28. D. Fishman, L. Ohana and N. Foucks, *Journal of Failure Analysis and Prevention*, 16 (2016) 1067.
29. R. Frost, *Spectrochimica Acta Part A: Molecular and Biomolecular Spectroscopy*, 59 (2003) 1195.
30. A. El-Etre and M. Abdallah, *Corrosion Science*, 42 (2000) 731.
31. M. Scherer, J. Westall and P.G. Tratnyek, *Corrosion Science*, 44 (2002) 1151.
32. M. Criado, S. Martínez-Ramirez and J. Bastidas, *Construction and Building Materials*, 96 (2015) 383.
33. M. Mennucci, E. Banczek, P. Rodrigues and I. Costa, *Cement & Concrete Composites*, 31 (2009) 418.
34. R. Villamil, P. Corio, S. Agostinho and J. Rubim, *Journal of Electroanalytical chemistry*, 472 (1999) 112.
35. N. ELDAKAR and K. Nobe, *Corrosion*, 33 (1977) 128.
36. A. Singh, A. Kumar and T. Pramanik, *Oriental Journal of Chemistry*, 29 (2013) 277.
37. P. Ejikeme, S. Umana, I. Alinnor, O. Onukwuli and M. Menkiti, *American Journal of Materials Science*, 4 (2014) 194.
38. J. Singh and D. Singh, *Corrosion Science*, 56 (2012) 129.
39. Y. El Mendili, J. Bardeau, N. Randrianantoandro, F. Grasset and J. Greneche, *The Journal of Physical Chemistry C*, 116 (2012) 23785.
40. S. Ofoegbu, T. Galvão, J. Gomes, J. Tedim, H. Nogueira, M. Ferreira and M. Zheludkevich, *Physical Chemistry Chemical Physics*, 19 (2017) 6113.
41. V. L'Hostis, D. Neff, L. Bellot-Gurlet and P. Dillmann, *Materials and Corrosion*, 60 (2009) 93.